CANCER BIOTHERAPY AND RADIOPHARMACEUTICALS
Volume 32, Number 7, 2017

DOI: 10.1089/cbr.2017.2253

Synthesis, Positron Emission Tomography Imaging, and Therapy of Diabody Targeted Drug Lipid Nanoparticles in a Prostate Cancer Murine Model

Patty Wong,[1] Lin Li,[2] Junie Chea,[2] Melissa K. Delgado,[2] Erasmus Poku,[2] Barbara Szpikowska,[2] Nicole Bowles,[2] Megan Minnix,[2] David Colcher,[2] Jeffrey Y.C. Wong,[1] John E. Shively,[2] and Paul J. Yazaki[2]

Abstract

The blood clearance of chemotherapeutic drugs such as doxorubicin (Dox) can be extended by incorporation into lipid nanoparticles (LNPs) and further improved by tumor targeting with antibody fragments. We used positron emission tomography (PET) imaging in a murine prostate cancer model to evaluate tumor targeting of LNPs incorporating Dox and antiprostate-specific membrane antigen (PSMA) diabodies. Dox-LNPs were generated by mixing or covalent attachment to water soluble distearoylphosphatidyl ethanolamine-polyethylene glycol $(DSPE\text{-}PEG)_{2000}$. Cu-64 PET imaging was performed with DOTA-conjugated Dox, PEG-LNP, or an anti-PSMA site-specific cysteine-diabody. Since the mixture Dox+PEG-LNP was unstable in serum, further studies utilized Dox covalently bound to LNP ± covalently bound DOTA-cys-diabody (cys-DB)-LNP. Blood clearance of covalent Dox-PEG-LNP was slower than Dox alone or Dox+PEG-LNP. PET imaging of ^{64}Cu-DOTA-Dox-PEG-LNP reached a maximum of 10% ID/g in tumors compared with 3% ID/g of ^{64}Cu-DOTA-Dox, due to the prolonged blood clearance. Mixing ^{64}Cu-DOTA-cys-DB-PEG-LNP with covalent Dox-PEG-LNP gave LNPs containing both drug and tumor targeting cys-DB. The mixed LNPs exhibited increased tumor uptake (15% ID/g) versus untargeted ^{64}Cu-DOTA-Dox-PEG-LNPs (10% ID/g) demonstrating feasibility of the approach. Based on these results, a therapy study with mixed LNPs containing cys-DB-LNP and either Dox-LNP or the antitubulin drug auristatin-LNP showed significant reduction of tumor growth with the auristatin-diabody-LNP mixture, but not the Dox-diabody-LNP mixture.

Keywords: diabody, doxorubicin, lipid nanoparticles, positron emission tomography, prostate cancer

Introduction

Lipid nanoparticles (LNPs) have an extensive history as drug delivery vehicles, with more than 15 agents approved and currently over 600 clinical trials that incorporate LNPs for cancer therapy.[1,2] Composed of a diverse set of natural or synthetic polymers, LNPs form small (10–300 nm in diameter) vesicles capable of encapsulating chemotherapeutics, providing improvements over traditional systemic drug delivery.[3] Advantages include increased antitumor activity, decreased off-target toxicity, enhanced solubility of hydrophobic drugs, limited drug degradation by serum proteases, improved intracellular delivery by membrane fusion, and prolonged pharmacokinetics compared with small molecules. Despite the many advantages, many challenges remain for improvement of this drug delivery system, including the need for specific and high tumor targeting, tumor uptake of the drug associated LNP, homogenous tumor penetration, formulation of multiple drug payloads, quantitation of tumor versus normal tissue uptake, and reduction of toxicity.

While liposomal formulations are widely used to entrap drugs, their preparation is time consuming and requires drug-specific procedures to introduce the drug into the liposome, a process that depends on the drug's charge and hydrophobic characteristics.[4,5] Polyethylene glycol (PEG)-LNPs are an attractive alternative to liposomes, since they can self-assemble into uniform-sized micelles under aqueous conditions.[6,7] Although many drugs may be incorporated into PEG-LNPs based

[1]Department of Radiation Oncology, City of Hope National Medical Center, Duarte, California.
[2]Department of Molecular Immunology, Beckman Research Institute, City of Hope, Duarte, California.

Address correspondence to: Paul J. Yazaki; Department of Molecular Immunology; Beckman Research Institute, City of Hope; 1500 East Duarte Road, Duarte, CA 91010-3000
E-mail: **pyazaki@coh.org**

on their charge and/or hydrophobicity, such preparations are often unstable under physiological conditions.[8] A good example is the slow loss of doxorubicin (Dox) from LNPs due to the effects of pH and Ca^{2+} on the electrostatic interaction between the positively charged drug and negatively charged phospholipid head group.[9] This problem may be addressed by covalent coupling of the drug to LNP derivatives.[3]

In the case of cancer therapeutics, both liposomal-drug and PEG-LNP drug mixtures depend on tumor accumulation based on the enhanced permeability retention effect that relies on the inherent leakiness of tumor vasculature over normal tissue.[10–13] In theory, tumor accumulation could be improved by the attachment of tumor targeting agents such as antibodies or antibody fragments. However, the use of targeted LNPs has had mixed results for tumor accumulation over what can be achieved by untargeted LNPs.[14] The use of targeted LNPs has been attempted with varying results based on the ligand-receptor system and size of the LNP.[15,16]

While the use of targeted liposomes for drug delivery has an extensive literature, on the whole, they perform no better than untargeted liposomes perhaps due to their >100 nm size.[17,18] PEG-LNPs that have a smaller molecular size (10–30 nm) are formed by the self-assembly of lipid hydrophilic and hydrophobic domains under aqueous conditions.[19] The block copolymer, distearoylphosphatidyl ethanolamine (DSPE)-PEG has been the cornerstone for micelle drug delivery.[6,19] Immunotargeted LNPs have demonstrated increased accumulation at the tumor site compared with liposomal formulations, again perhaps due to their smaller molecular size.[20]

Given the attraction of self-assembled PEG-LNPs over the rather tedious preparation of liposomes, we have selected DSPE-PEG micelles for evaluating targeted drug PEG-LNP mixtures and covalent drug-PEG-LNPs in a prostate cancer model.[21] Prostate cancer was chosen as a model system due to the availability of excellent targeting antibodies to prostate-specific membrane antigen (PSMA), an antigen found in the majority of prostate tumors.[22]

Radionuclide imaging, specifically positron emission tomography (PET) provides an important noninvasive tool for the *in vivo* quantitative assessment of nanoparticle targeting capabilities in cancer therapy.[23–26] In a recent study, we utilized an anti-PSMA single-chain (scFv) antibody to show that targeted LNPs exhibited a twofold increase in tumor uptake compared with the scFv alone or the untargeted LNP micelle formulation by Cu-64 PET imaging.[27] This study extends that finding by incorporation of a bivalent anti-PSMA diabody and a chemotherapy drug-LNP payload. For the initial experiments Dox was chosen as a model drug for its inherent fluorescence that allows quantitation of tumor uptake.[28]

To accomplish this approach, DOTA-conjugated Dox and DOTA-anti-PSMA diabodies were generated, the products incorporated into PEG-LNPs and labeled with Cu-64. We demonstrate in this study that separate LNPs, one carrying drug and one carrying anti-PSMA diabody, can be mixed forming a homogeneous LNP that gives superior tumor targeting compared with the individual LNPs. Based on these results, we performed a therapy study in mice bearing PSMA-positive prostate tumor xenografts comparing two covalent drug-LNPs mixed with covalently bound anti-PSMA cys-diabody (cys-DB). The results show the feasibility of the approach along with significant tumor reduction by one of the drug-cys-DB-LNP mixtures compared with drug-free LNP controls or drug-cys-DB controls.

Materials and Methods

Chemicals

Chemicals were purchased from commercial sources with >98% purity.

Electron microscopy, size-exclusion chromatography, and light-scattering measurements

Electron microscopy (EM) was performed on an FEI Tecnai 12 transmission electron microscope equipped with a Gatan Ultrascan 2K CCD camera. LNP samples were applied to a glow-discharged 300 mesh Formvar–carbon copper EM grid and stained with 2% uranyl acetate or Nano-W®. Light scattering was performed on ZetaPALS (Brookhaven Instruments, Corp.).

LNPs were purified on an AKTA Purifier (GE Healthcare) using size-exclusion chromatography (SEC), on a Superdex-200 10/300 GL column (GE Healthcare) at a flow rate of 0.5 mL/minute in phosphate-buffered saline (PBS).

The average size of an LNP preparation was ~20 nm by light scattering, 15–30 nm by EM, and a retention time of 17.5 minutes on SEC.

Anti-PSMA diabody

An anti-PSMA cys-DB based on the anti-human PSMA monoclonal antibody J591[29] was constructed in the variable heavy to variable light domain (VL) orientation joined by a glycine/serine (GGGSGGGG) amino acid linker with a carboxy-terminal L6 linker (SAKTTP) and a six histidine (his6) tag for purification. For site-specific conjugation, four internal cysteines were introduced into the VL framework to form two disulfide loops (Supplementary Fig. S1; Supplementary Data are available online at www.liebertpub.com/cbr) as previously described for a different diabody.[30]

The complementary DNA encoding the diabody was cloned into the pEE12.4 plasmid (Lonza Group, Ltd., Basil, Switzerland) and transiently expressed using the mammalian Expi293™ Expression system (Life Technologies, Grand Island, NY). The culture supernatants were affinity purified by immobilized metal affinity chromatography using a 5 mL Ni-NTA superflow cartridge following the manufacture's protocol (Qiagen, Germantown, MD). The diabody was further purified by ceramic hydroxyapatite, Type I (Bio-Rad Laboratories, Hercules, CA),[31] resulting in a high yield of 100 mg per L of culture. For radiometal labeling, the diabody was conjugated with *N*-hydroxysuccinimide 1,4,7,10-tetraazacyclododecane-1,4,7,10-tetraacetic acid (NHS-DOTA, Macrocyclics, Dallas, TX) as previously described.[32]

Preparation of Dox-HCl LNP mixtures

DSPE-$mPEG_{2000}$ (Avanti Polar Lipids, Alabaster, AL; 12.6 mg in 320 μL of saline) was mixed at a 1- to 1-molar ratio with Dox HCl. The incubation was performed under argon for 60 minutes at 60°C. When the mixture was purified by SEC, a major peak containing the Dox-LNP separated from free Dox was obtained. The percent Dox in the Dox-LNP mixture ranged from 60% to 90% by monitoring the fluorescence of Dox (excitation 480 nm, emission 550 nm) based on known standards in a flow through detector (FP 2020 Plus; Jasco, Inc., Easton, MD).

Preparation of covalent Dox-LNP

DSPE-PEG_{2000}-CO_2H (Avanti Polar Lipids; 4.84 mg in 484 μL of saline) was reacted with a 2-molar excess of sulfo-NHS), a 2-molar excess of 1-Ethyl-3-(3-dimethylaminopropyl) carbodiimide (EDC) and 2-molar excess of Dox HCL. The reaction was performed under gentle agitation, overnight at room temperature (RT). The product was purified by SEC and the percent incorporation calculated by fluorescence (see Preparation of Dox-HCl LNP mixtures). The major peak containing 25% covalently bound Dox was used for further studies (Supplementary Fig. S2A).

Preparation of Dox-DOTA

Dox HCL (Sigma; 2.7 mg in 2.0 mL of MeOH) was reacted 1:1 molar ratio of DOTA-NHS and 1.2 molar excess of solid sodium carbonate under gentle agitation overnight at RT. The product was purified by reverse phase (RP) high-performance liquid chromatography (HPLC). RP conditions were a CN column, (Luna 3u CN 100A 30 × 4.60 mm; Phenomenex, Torrance, CA) run on an AKTA Purifier using a gradient from 100% 0.1% trifluoroacetic acid to 100% acetonitrile over 30 minutes. The purified product (50% yield) analyzed by electrospray ionization mass spectrometry (ESI-MS) performed on a Finnigan LTQ™ (ThermoElectron, San Jose, CA) providing these correct masses: obs m/z = 930.36, calc. m/z = 930.5.

Preparation of Dox-DOTA-LNP

DSPE-PEG_{2000}-maleimide (Avanti Polar Lipids; 0.5 mg in 100 μL of PBS) was reacted with a twofold molar excess of DOTA-monoacetamidoethanethiol (DOTA-EtSH) under gentle agitation, overnight at 37°C. Excess DOTA-EtSH was removed by a spin column, and the product was purified by SEC. DOTA-LNP was activated with a twofold excess of EDC/Sulfo-NHS for 30 minutes at pH 4.5, the pH raised to 7.0, and a twofold excess of Dox-HCl was added and allowed to react overnight (Supplementary Scheme1 and Supplementary Fig. S2B). Dox-DOTA-LNP was purified by SEC to give two poorly separated peaks at 16 and 18 minutes. The percent incorporation of Dox was 50% for each peak using fluorescence intensity at 550 nm and ultraviolet at 280 nm.

Preparation of DOTA-cys-DB-LNP

DSPE-PEG_{2000}-NH_2 [Avanti Polar Lipids; 6 mg in 300 μL of dichloromethane (DCM)] was reacted with a 10 molar excess of bromoacetylbromide and 10 molar excess of triethylamine (TEA). The product was evaporated to dryness, then resuspended in 1 mL water, and purified by SEC. Reduced DOTA-cys-DB (0.364 mg in 170 μL of PBS) was reacted with an 11.5-molar excess of DSPE-PEG_{2000}-acetBr (0.5 mg in 99 μL of PBS) overnight at 37°C. The product was purified by SEC-HPLC (Supplementary Fig. S2C).

Preparation of DOTA-cys-DB-LNP plus Dox-LNP

DSPE-PEG_{2000}-CO_2H (17.5 mg in 900 μL of DCM) was reacted with a 2 molar excess of 1 M *N,N'*-Dicyclohexylcarbodiimide (DCC), 2 molar excess of 0.5 M hydroxybenzotriazole (HOBt), and 1:1 molar ratio of Dox HCL (3.85 mg) overnight at RT. The product was dialyzed in a Slide-A-Lyzer (Thermo Fisher Scientific, Grand Island, NY) 2000 molecular weight cut-off (MWCO) to remove excess reagents. The purified Dox-LNP was quantitated by fluorescence intensity as 65% conjugation yield. DSPE-PEG_{2000}-NH_2 (13 mg in 650 μL of DCM) was reacted with a 10 molar excess of bromoacetylbromide with a 10-molar excess of TEA. The product was evaporated to dryness and purified by RP-HPLC. Reduced DOTA-cys-DB (0.728 mg in 170 μL of PBS) was reacted with an 11.5 molar excess of DSPE-PEG_{2000}-acetBr (0.5 mg in 99 μL of PBS) overnight at 37°C. The product was purified by SEC-HPLC. DSPE-PEG_{2000}-COOH-Dox was mixed with DSPE-PEG_{2000}-cys-DB-DOTA overnight at 37°C (Supplementary Fig. S2D).

Preparation of MMAE-DB, MMAE-LNP, and Dox-LNP for therapy

MMAE (Levena Biopharma, San Diego, CA; 279 μmole in 1.5 mL of dry Dimethylformamide (DMF)) was reacted with 56 μmole of bromoacetic anhydride (solid) under gentle agitation, overnight at RT. The product, bromoacetamido-MMAE (BrAc-MMAE), was purified by RP-HPLC (Gemini C18, 2.1 × 200 mm, yield 84%) and its mass determined by ESI-MS (obs. m/z = 838.36, calc. m/z = 838.88).

BrAc-MMAE (25 mg, 3 μmole) in 0.875 mL of dry DMF was reacted with a 2 molar excess of cysteamine and 10 molar excess of solid sodium carbonate for 2 hours at RT. The product was purified by RP-HPLC (Gemini C18, 2.1 × 200 mm, yield 40%) and analyzed by MS (obs. m/z = 835.64, calc. m/z = 835.03). DSPE-PEG_{2000}-COOH (20 mg, 7 μmole) in 2 mL of DCM was activated with DCC/HOBt as above mentioned and reacted with a 1:1 molar ratio of NH_2-$(CH_2)_2S(CH_2)$CO-MMAE in 0.7 mL of dimethyl sulfoxide (DMSO) under gentle agitation, overnight at RT. The product was dialyzed (2000 MWCO) versus PBS to remove excess reagents and purified by SEC-HPLC (single peak at 20 minutes). The incorporation of MMAE into the final product was calculated by NMR as 45%.

DSPE-PEG_{2000}-COOH (40 mg, 14 μmole) in 2 mL of DCM was activated with a 2 molar excess of DCC and HOBt and reacted with 1:1 molar amount of Dox-HCl under gentle agitation, overnight at RT. The product was dried to remove DCM, dialyzed (2000 MWCO) versus PBS to remove excess reagents. The product was purified by SEC (single peak at 20 minutes) and the incorporation of Dox calculated by fluorescence (ex = 480 nm, em = 550 nm) as 6.5%.

Radiolabeling

Dox-DOTA-LNP, DOTA-cys-DB-PEG-LNP, and DOTA-Dox were radiolabeled with Cu-64 to obtain a final specific activity of 3–10 μCi per μg as previously described.[33] In brief, the DOTA-constructs were adjusted to 0.25 M ammonium acetate pH 5.5, ~250 μg were incubated with 2.5 MCi of ^{64}CuCl (Isotope Production group, Washington University Medical School in St. Louis, St Louis, MO) at 43°C for 45 minutes, adjusted to 1 mM diethylenetriaminepentaacetic acid, and incubated for 10 minutes at RT. Radiolabel incorporation was >75% as measured by instant thin layer chromatography. The ^{64}Cu-DOTA-constructs were purified on a SEC Superdex 200 column immediately before injection into animals.

The radiolabeled DOTA-cys-DB-LNP was analyzed for immunoreactivity by coincubation with soluble PSMA (R&D Systems, Minneapolis, MN). In a liquid phase assay radiolabeled immuno-LNP were incubated with 20 equivalents by mass of antigen and the resultant complex analyzed by analytical SEC. The immunoreactivity was determined by integrating the area on the SEC radiochromatogram and calculating the percentage of radioactivity shifting to higher

molecular weight, consistent with the complexation of the immune-LNP with its cognate antigen.

PET imaging, terminal tissue analysis, and therapy studies in tumor-bearing mice

All animal handling was done in accordance with IACUC protocols 91037 and 12031 approved by the City of Hope Institutional Animal Care and Use Committee. Male 6- to 8-week-old Non-obese diabetic severe combined immune deficiency (NOD/SCID) mice (average size 25 g) were injected in the preputial fat pad with mixture of Matrigel (Corning, Inc., Corning, NY) and LNCaP human prostate cancer cells (No. CRL-1740; ATCC, Manassas, VA) at a ratio of 7:3 v/v (3×10^6 cells in 200 μL). After 4–8 weeks, the tumor masses were in the range of 0.2–0.6 g.

In individual experiments, ^{64}Cu-DOTA-cys-DB-LNP, ^{64}Cu-DOTA-Dox-LNP, and ^{64}Cu-DOTA-Dox were injected (100 μCi in 50–200 μL/animal) via tail vein with two mice per group. The PET imaging was performed at set time points using an Inveon microPET system (Siemens, Malvern, PA). At the last time point, computed tomography (CT) imaging was performed; the CT and PET images were aligned for coregistration.

After the final images were taken, a terminal tissue analysis is performed to calibrate the quantitation of the PET images. The two mice per group were euthanized, necropsy performed, and organs weighed and counted for radioactivity. The radioactivity has been corrected for background and radioactive decay from the time of injection, allowing organ uptake to be reported as percent injected dose per gram (% ID/g).

Two therapy studies were conducted. One tested the effect of cys-DB-conjugated LNPs mixed with drug-conjugated LNPs and the other with drug-conjugated to cys-DB alone. In the study with mixed LNPs, cys-DB-LNP was prepared as above mentioned and mixed 1:1 (w/w) with either Dox-LNP or MMAE-LNP (see Preparation of MMAE-DB, MMAE-LNP and Dox-LNP for therapy). Male NOD/SCID mice bearing human prostate LnCAP tumors (3×10^6 cells s.c. treatment started at 100 mm^3) were divided into three groups (7–8 mice per group), one receiving saline (no treatment), one receiving mixed LNPs with DB-LNP + Dox-LNP, and one receiving mixed LNPs with DB-LNP + MMAE-LNP. The total injection volume was 0.2 mL comprising 300 μg of LNP, 10 μg of drug, and 15 μg of cys-DB. The mice were injected i.v. twice a week for 4 weeks and tumor measurements performed twice a week.

The second therapy study was a follow-up to the first. Cys-DB (7.0 mg, 140 nmol in 1 mL of PBS) was reduced with a 30-molar excess of tris(2-carboxyethyl)phosphine (TCEP) for 2 hours under Ar, excess TCEP removed by a spin column, then reacted with a 20-molar excess of BrAc-MMAE in DMF overnight at RT, and dialyzed versus PBS. The product gave a single peak at 29 minutes. NOD/SCID mice bearing LnCAP tumors (100 mm^3) were treated with 0, 2.5 or 5.0 mg/kg of conjugate in 0.05 or 0.1 mL of PBS twice a week intraperitoneal (i.p.) for 4 weeks. Controls included treatment with cys-DB alone (5 mg/kg).

Results and Discussion

Generation and evaluation of noncovalent and covalent Dox-PEG-LNPs

The copolymer DSPE-PEG$_{2000}$ is soluble in PBS above its critical micelle concentration and gives a single peak on SEC (Fig. 1A), demonstrating that it spontaneously forms a homogeneous LNP under aqueous conditions. The particle size was about 30 nm as analyzed by light scattering or EM. When DSPE-mPEG$_{2000}$ was mixed at a 1:1 molar ratio with Dox-HCl in saline for 30 minutes at RT and purified by SEC (Fig. 1B), the LNP size was retained along with incorporation of 60%–90% of the admixed Dox-HCl.

However, the stability of DSPE$_{2000}$ + Dox mixtures has been shown to be unstable in serum due to the combined effects of pH and Ca^{2+}. An increase in pH to 7.0 leads to a decrease in the positive charge on Dox, while the complexation of Ca^{2+} with the negatively charged phosphate head group competes with its interaction with positively charged Dox.[9] Indeed, when Dox + LNP (initial pH of 4.5) was incubated with mouse serum for increasing times, Dox was rapidly lost from the LNP and bound to serum albumin (Fig. 1C,D). Figure 1C SEC analysis shows the majority of the Dox fluorescence emission (solid line) has shifted to the retention time of albumin (dotted line) compared with starting material retention time in Figure 1B.

In addition, we noted that Dox-HCl rapidly precipitates in normal saline (unadjusted pH = 2–3), when the solution is adjusted to pH 7.0 (data not shown). Thus, it is likely that when free Dox-HCl is infused directly into the blood stream, a combination of precipitation and transfer to serum albumin occurs, explaining its rapid clearance from the blood.[34–36]

Injection of equivalent doses of free Dox-HCl or Dox + LNP mixture into tumor-bearing animals and quantitation of tumor uptake at 1 hour postinjection revealed roughly equivalent amounts of Dox incorporation into tumor (Fig. 2), suggesting that the Dox + LNP formulation was unstable in serum.

Since the Dox + LNP preparation rapidly lost its bound Dox under physiological conditions, we investigated methods for the covalent attachment of Dox to a functionalized DSPE-PEG$_{2000}$ reagent. The first derivative tested was DSPE-PEG$_{2000}$-COOH, containing a pendant carboxyl group. When this group was converted to an active ester using sulfo-NHS/EDC activation chemistry and reacted with the free amino group of Dox, the LNP incorporated about 50% Dox as determined by monitoring the fluorescence of the purified product on SEC (Supplementary Fig. S3).

Notably, the Dox-LNP gave a single symmetric peak on SEC, suggesting that the conjugated Dox did not affect micelle formation or its size. When the Dox-LNP was injected into tumor-bearing animals and compared with an equivalent amount of free Dox or the Dox + LNP mixture, the amount of Dox found in tumors 1-hour postinjection was roughly equivalent (Fig. 2). Thus, at least at the 1-hour time point measurement, all three preparations, free Dox-HCl, Dox+ LNP, and Dox-LNP, had similar tumor uptake.

Although the amount of Dox in a given tissue can be determined by extraction and fluorescent measurement, this analysis suffers from low sensitivity (variable extraction efficiency) and high-fluorescent tissue quenching, especially in blood. Therefore, we explored the possibility of following these preparations *in vivo* by making chelate conjugates of the Dox preparations, radiolabeling with Cu-64, and PET imaging, followed by terminal tissue analysis. When the amino group of Dox-HCl was conjugated to an active ester derivative of DOTA, the derivative was quantitatively radiolabeled with Cu-64 to a specific activity of 3 μCi/μg and 22 μg injected into tumor-bearing animals. As expected,

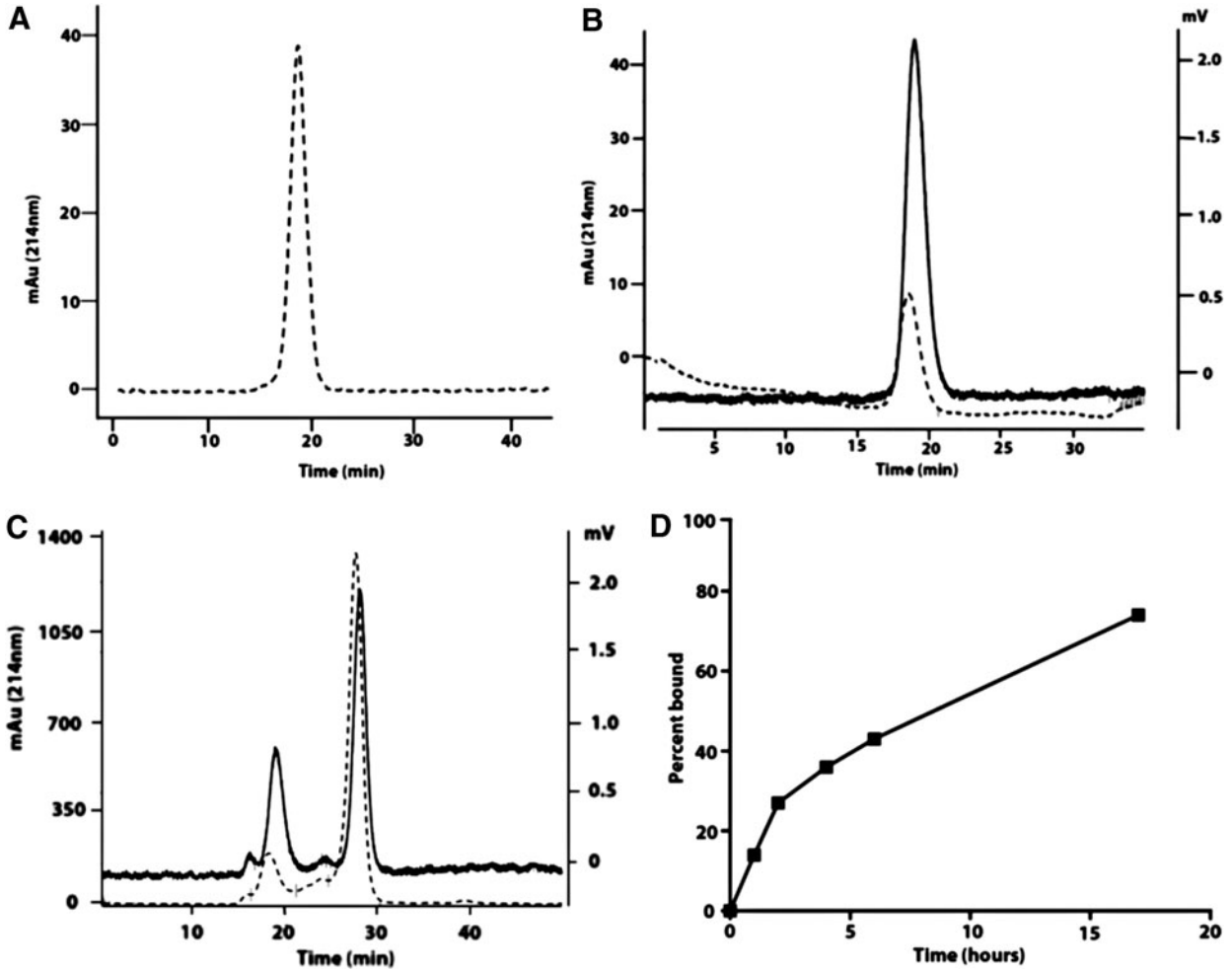

FIG. 1. Analysis of DSPE-PEG$_{2000}$ plus Dox-HCl mixture by SEC and its serum stability. **(A)** SEC analysis of DSPE-mPEG$_{2000}$ (*dotted line* A_{214}nm). **(B)** SEC analysis of DSPE-mPEG$_{2000}$ mixed with Dox-HCl (*dotted line* A_{214}nm, *solid line* fluorescence emission at 560 nm). **(C)** SEC analysis of DSPE-mPEG$_{2000}$ + Dox HCl incubated with serum for 12 hours (*dotted line* A_{214}nm, *solid line* fluorescence emission at 560 nm). **(D)** Plot of percent Dox HCl bound to serum albumin (peak at 28 minutes in **(B)** over time. Dox, doxorubicin; DSPE-PEG, distearoylphosphatidyl ethanolamine-polyethylene glycol; SEC, size-exclusion chromatography.

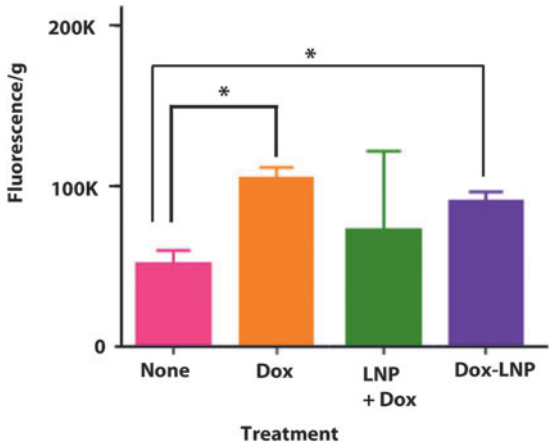

FIG. 2. Uptake of Dox into LnCAP tumors. NOD/SCID mice bearing LnCap tumors were injected with saline (none) or Dox-HCL preparations (100 mg/kg) as indicated. Animals were euthanized 1 hour later, Dox extracted as described in Materials and Methods, the fluorescence was read at 560 nm, and the results normalized to tumor weight (*$p < 0.005$). Dox, doxorubicin; LNP, lipid nanoparticle; NOD/SCID, non-obese diabetic severe combined immune deficiency.

^{64}Cu-DOTA-Dox cleared rapidly from the blood into the liver, kidneys, and bladder, with terminal uptake (4 hours) in the liver and bladder (Fig. 3A). As measured by PET imaging, maximum uptake in the tumor was observed at 4 hours when normal tissue background was reduced. The terminal tissue analysis performed at 4 hours showed a tumor uptake of about 3% ID/g (Fig. 3B), correlating to about 0.12 μg of Dox accumulation in the tumor. The tumor to blood ratio at 4 hours was about 1.5, close to the limit of detection for PET imaging. Thus, DOTA-Dox, such as Dox itself, clears rapidly from the blood, suggesting that higher doses would be required to effect tumor therapy.

To perform PET studies on Dox-LNPs, we first prepared DOTA-LNP starting from DSPE-PEG$_{2000}$-maleimide, containing a thiol reactive moiety for conjugation to a thiol derivative of DOTA (DOTA-monoacetamidoethanethiol). A carboxyl group of the terminal DOTA moiety was then activated with EDC-sulfo-NHS, followed by the addition of Dox-HCl to generate Dox-DOTA-LNP (Scheme S1 and Supplementary Fig. S2B). SEC analysis of Dox-DOTA-LNP before and after radiolabeling with Cu-64 revealed two poorly separated peaks, eluting at 16 and 18 minutes, suggesting the presence of two different sizes of micelle with equivalent amounts of Dox (Supplementary Fig. S4). The

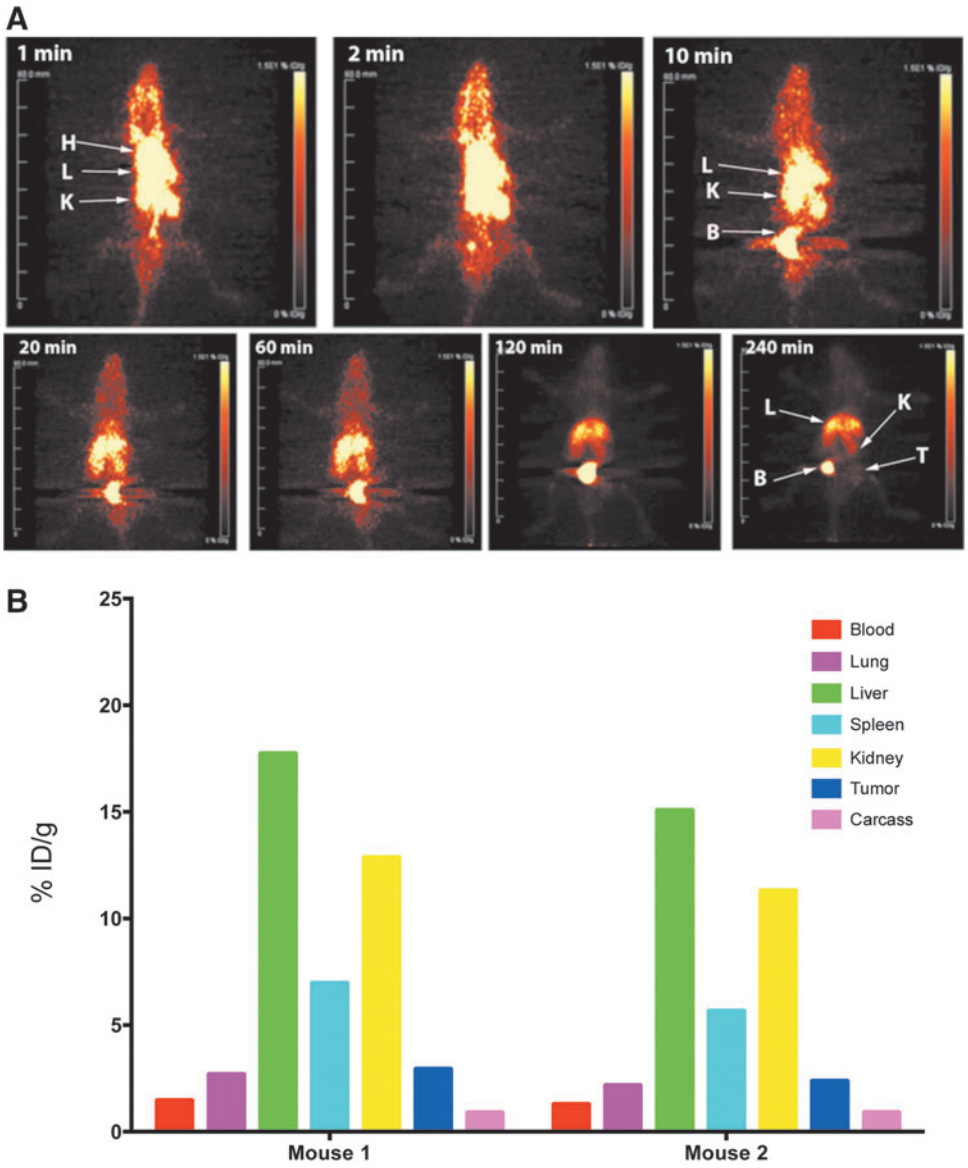

FIG. 3. PET imaging and terminal tissue analysis of Cu-64-DOTA-Dox in NOD-SCID mice bearing PSMA-positive LNCap prostate tumors. **(A)** PET imaging of Cu-64-DOTA-Dox. ^{64}Cu-DOTA-Dox (20 μCi/6.6 μg) was injected into two male NOD/SCID mice per group bearing LnCap tumors and PET imaged over 4 hours. Although frames for specific time points are shown for a single mouse, the results were similar for a second mouse with a similar size tumor. At 1 minute, the main organs imaged were heart (H), liver (L), and kidneys (K). The uptakes above the heart are the jugular veins. Uptake in the bladder **(B)** was observed as early as 2 minutes with substantial urinary excretion into the bladder until the last time point at 240 minutes. Tumor (T) uptake was barely visualized. **(B)** Terminal tissue analysis of Cu-64-DOTA-Dox. After the final PET image was acquired, mice were euthanized, tissues weighed and counted for radioactivity for quantitative tissue analysis to calibrate the PET images. The data are expressed for the two individual mice as % ID/g for major organs at the terminal time point of 4 hours. Dox, doxorubicin; NOD/SCID, non-obese diabetic severe combined immune deficiency; PET, positron emission tomography; PSMA, prostate-specific membrane antigen.

two peaks were combined and injected into tumor-bearing animals for PET imaging and terminal tissue analysis. As shown in Figure 4A and B, while high kidney and liver uptake were still observed, there was substantial uptake (10% ID/g) in the tumor. Compared with ^{64}Cu-DOTA-Dox, there was a fourfold increase in tumor uptake for ^{64}Cu-Dox-DOTA-LNP, due to the anticipated slower blood clearance of the micelle preparation. Nanoparticles of various composition and sizes are able to cross the blood–brain barrier.[37] During the short time course of this study, however, brain uptake was below 1% ID/g and not reported. The blood clearance of ^{64}Cu-Dox-DOTA-LNP is shown in Supplementary Figure S5. Thus, the covalent conjugation of Dox to LNP is a reasonable strategy for improving tumor uptake of Dox compared with Dox alone that clears rapidly from the blood.

Preparation and evaluation of targeted PEG-LNPs and mixed drug-targeted PEG-LNPs

Since antibody-targeted LNPs have the potential to increase tumor uptake, we evaluated mixtures of antibody-targeted PEG-LNPs with Dox-PEG-LNPs to determine if the antibody-targeted PEG-LNPs were capable of increasing tumor delivery of Dox. The obvious advantage of this approach is that separate drug and antibody LNPs could be synthesized, characterized, and then mixed according to the nature of the tumor target in terms of antigen expression and drug sensitivity. A humanized anti-PSMA cys-DB (Supplementary Fig. S1) was genetically engineered with site-specific disulfide loops for thiol chemistry attachment similar to the CC-49 cys-DB.[29] For PET imaging, DOTA was conjugated to the cys-DB by active ester chemistry and characterized by SEC (Fig. 5A). The resulting DOTA-cys-DB was radiolabeled with Cu-64 and shown to retain 100% immunoreactivity against soluble PSMA (Supplementary Fig. S1).

When the internal disulfide loops on the DOTA-cys-DB were reduced with TCEP and the excess TCEP removed by spin column, the exposed cysteines were reacted with the BrAc derivative of DSPE-PEG$_{2000}$-NH$_2$, as described in Materials and Methods. The resulting DOTA-cys-DB-LNP gave two peaks eluting at 16 and 18 minutes on SEC (Fig. 5B), again indicating that two different sizes of LNPs

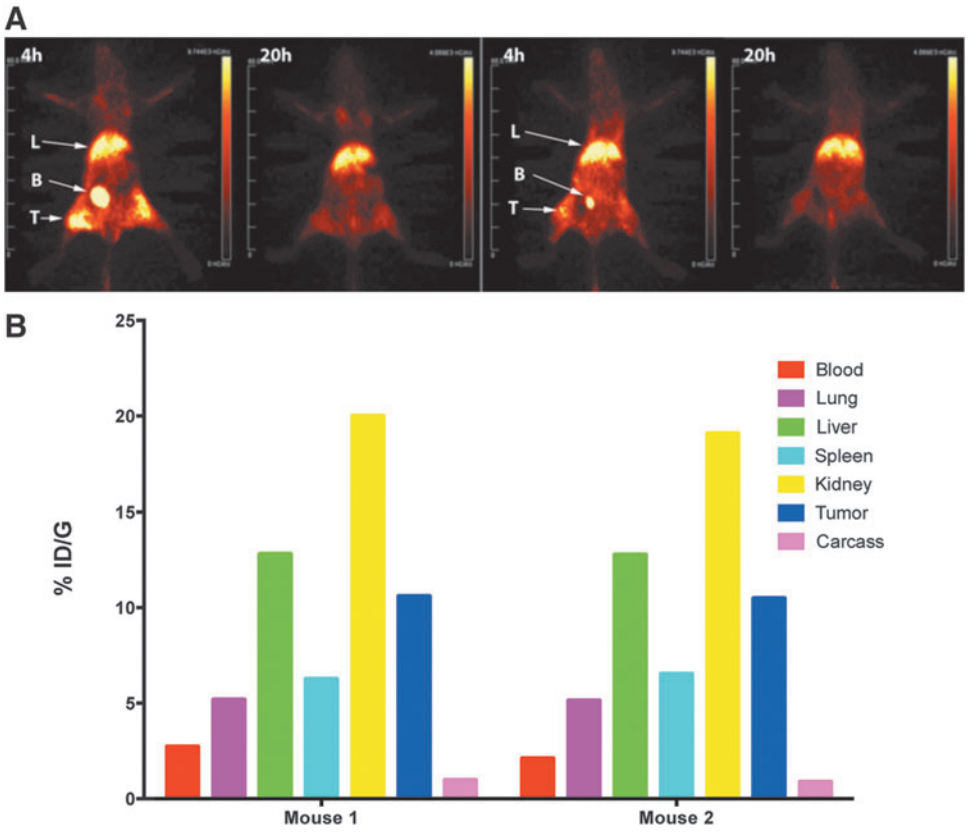

FIG. 4. PET imaging and terminal tissue analysis of Dox-^{64}Cu-DOTA-LNP in NOD-SCID mice bearing PSMA-positive LNCap prostate tumors. **(A)** PET imaging of ^{64}Cu-DOTA-Dox-LNP. Dox-^{64}Cu-DOTA-LNP was injected into two male NOD/SCID mice bearing LnCap tumors and PET imaged at 4 and 20 hours. **(B)** Terminal tissue data of Dox-^{64}Cu-DOTA-LNP. After the final PET image was acquired, mice were euthanized, tissues weighed and counted for radioactivity for biodistribution analysis. The data are expressed for the two individual mice as % ID/g for major organs at the terminal time point of 20 hours. Dox, doxorubicin; LNP, lipid nanoparticle; NOD/SCID, non-obese diabetic severe combined immune deficiency; PET, positron emission tomography; PSMA, prostate-specific membrane antigen.

were formed as with the Dox-DOTA-LNP. The two peaks were radiolabeled with Cu-64 and separately injected into tumor-bearing animals to determine if the difference in apparent size would lead to different tumor and normal tissue uptake. PET imaging of the two preparations (Fig. 6) and terminal tissue analysis (Fig. 7) demonstrated equivalent results, suggesting that the apparent size difference had no effect on either tumor or nontarget tissue uptake.

To study the effect of mixing LNPs to allow combined antibody targeting and drug delivery in a LNP format, DOTA-cys-DB-LNP was mixed 1:1 (w/w) with Dox-LNP. When the resulting mixture was analyzed by transmission electron microscopy (TEM) and compared with Dox-LNP alone, the average size of micelles increased from 16 nm (Dox-LNP alone) to 20 nm, indicating that the resulting mixture was homogeneous in terms of drug and cys-DB incorporation (Supplementary Fig. S6). When the mixture was radiolabeled with Cu-64 and injected into tumor-bearing animals, tumor uptake was observed as early as 2 hours by PET imaging (Fig. 8A). The terminal tissue analysis at 19 hours demonstrated an average tumor uptake of 15% ID/g (Fig. 8B), an increase of 33% over that of Dox-LNP alone. As before, the liver and kidney were the major nontumor organs with high uptake.

Therapy with targeted mixed drug LNPs

Having demonstrated an improvement of tumor targeting with a mixture of LNPs with Dox plus cys-DB over that of Dox-LNPs alone, we were interested in demonstrating a therapeutic response. Although we had selected Dox as a model drug for conjugation to LNPs because it was easy to follow by fluorescence, we were also interested in other, more clinically relevant drugs, such as auristatin that has been shown to be effective in antibody-drug conjugates (ADCs).[38–40] Therefore, we synthesized an auristatin-LNP derivative (MMAE-LNP) and mixed it with cys-DB-LNPs to compare it with Dox-LNP mixed with cys-DB-LNPs in the treatment of NOD/SCID mice bearing LnCAP tumors. Compared with controls (cys-DB-LNP) or mixed LNP with Dox-LNP, the mixed LNP with MMAE-LNP led to significant tumor reduction (Fig. 9A). Although this result was encouraging, we considered the possibility that a direct conjugate of MMAE to cys-DB may also be effective. Therefore, this conjugate was prepared and a second therapy study performed using cys-DB as a control. As shown in Figure 9B, treatment with the MMAE-cys-DB at two dose levels had no effect on tumor growth, confirming that the drug therapy was more effective in the mixed LNP format.

Not unexpectedly, the MMAE-LNP plus cys-DB-LNP therapy was accompanied by modest general toxicity as shown by loss of weight in the treated versus control mice (Supplementary Fig. S7). Since we observed substantial liver uptake of LNPs (Fig. 8) and the main normal tissue target of MMAE is the liver,[38] we suspected liver toxicity was the cause of the weight loss. Indeed, a liver panel was consistent with this idea (data not shown). Despite this side effect, the treated mice began to regain weight after the treatment was discontinued, suggesting a reversible toxicity.

Conclusion

Conventional delivery of chemotherapeutic drugs suffers from rapid blood clearance and poor tumor targeting, leading to

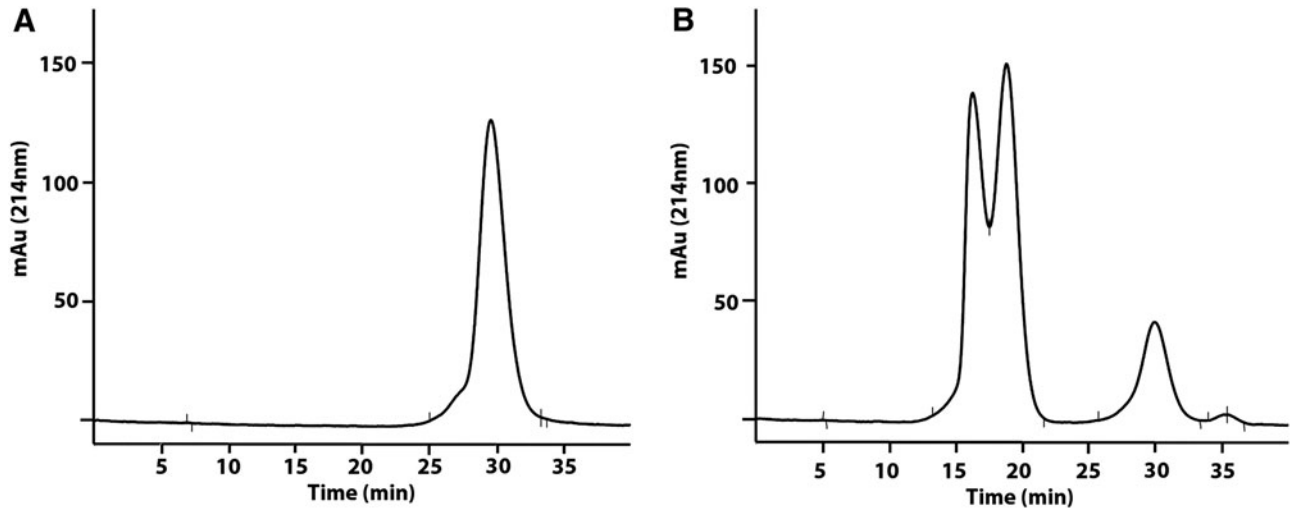

FIG. 5. SEC purification of DOTA-cys-DB-LNP. **(A)** SEC analysis of DOTA-anti-PSMA diabody (DOTA-cys-DB). A major peak was observed at 30 minutes. **(B)** Conjugation of reduced DOTA-cys-DB to the BrAc derivative of DSPE-PEG_{2000}-NH_2 (LNP) and purification by SEC. The peaks at 16 and 18 minutes correspond to DOTA-cys-DB-LNP and the peak at 30 minutes to unconjugated DOTA-cys-DB. cys-DB, cys-diabody; Dox, doxorubicin; DSPE-PEG, distearoylphosphatidyl ethanolamine-polyethylene glycol; LNP, lipid nanoparticle; PSMA, prostate-specific membrane antigen; SEC, size-exclusion chromatography.

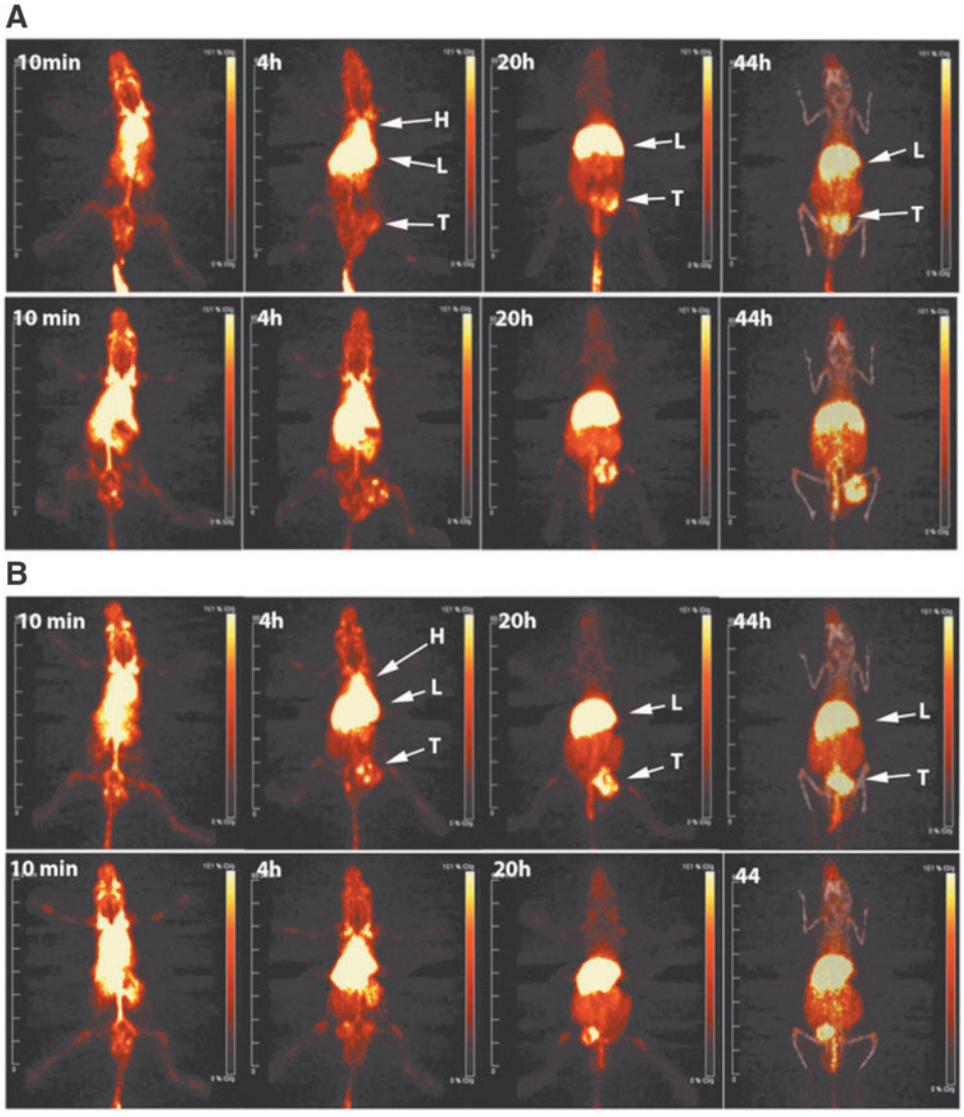

FIG. 6. PET imaging of ^{64}Cu-DOTA-cys-DB-LNP. The DOTA-cys-DB-LNP preparation was radiolabeled with Cu-64 and purified by SEC, yielding two LNP peaks eluting at 16 and 18 minutes. Each preparation was injected into two male NOD/SCID mice bearing LnCap tumors and serial PET imaged over 44 hours. **(A)** Representative PET imaging of ^{64}Cu-DOTA-cys-DB-LNP peak 1 (16 minutes) over time. Major organs imaged were heart (H), liver (L), and tumor (T). **(B)** Representative PET imaging of ^{64}Cu-DOTA-cys-DB-LNP peak 2 (18 minutes) over time. At the last time point, computed tomography imaging was performed and overlaid on the PET image. cys-DB, cys-diabody; LNP, lipid nanoparticle; NOD/SCID, non-obese diabetic severe combined immune deficiency; PET, positron emission tomography; SEC, size-exclusion chromatography.

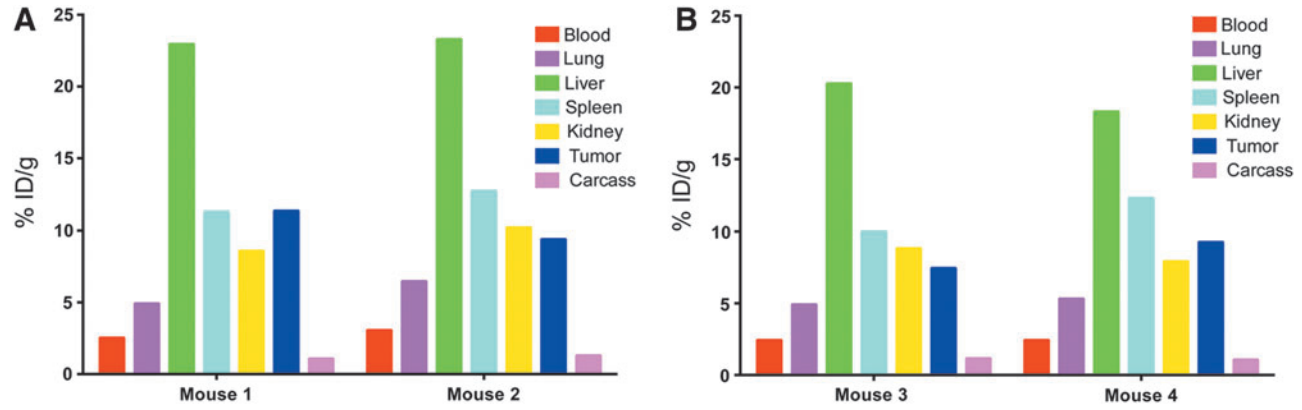

FIG. 7. Terminal tissue analysis of ^{64}Cu-DOTA-DB-LNPs. After the final PET image, terminal tissue analysis of ^{64}Cu-DOTA-cys-DB-LNP Peak 1 **(A)** and Peak 2 **(B)** was obtained (Fig. 6). For each peak, the two mice were euthanized, tissues weighed and counted for radioactivity for quantitative tissue uptake. The data are expressed for the individual mice as % ID/g for major organs at the terminal time point of 40 hours. cys-DB, cys-diabody; LNPs, lipid nanoparticles.

high normal tissue toxicity. In theory, the rapid clearance problem can be solved by incorporating the drugs into slower clearing LNPs, while the tumor targeting issue can be addressed by conjugating antibody fragments to the LNP. To achieve the goal of drug-targeted LNPs, each of these steps needs to be separately optimized using quantitative *in vivo* models. We have approached that problem by performing PET imaging at each stage of the optimization in a model of prostate cancer. We selected Dox as a model drug, not only because it is used in first or second line chemotherapy of many cancers but also because it is

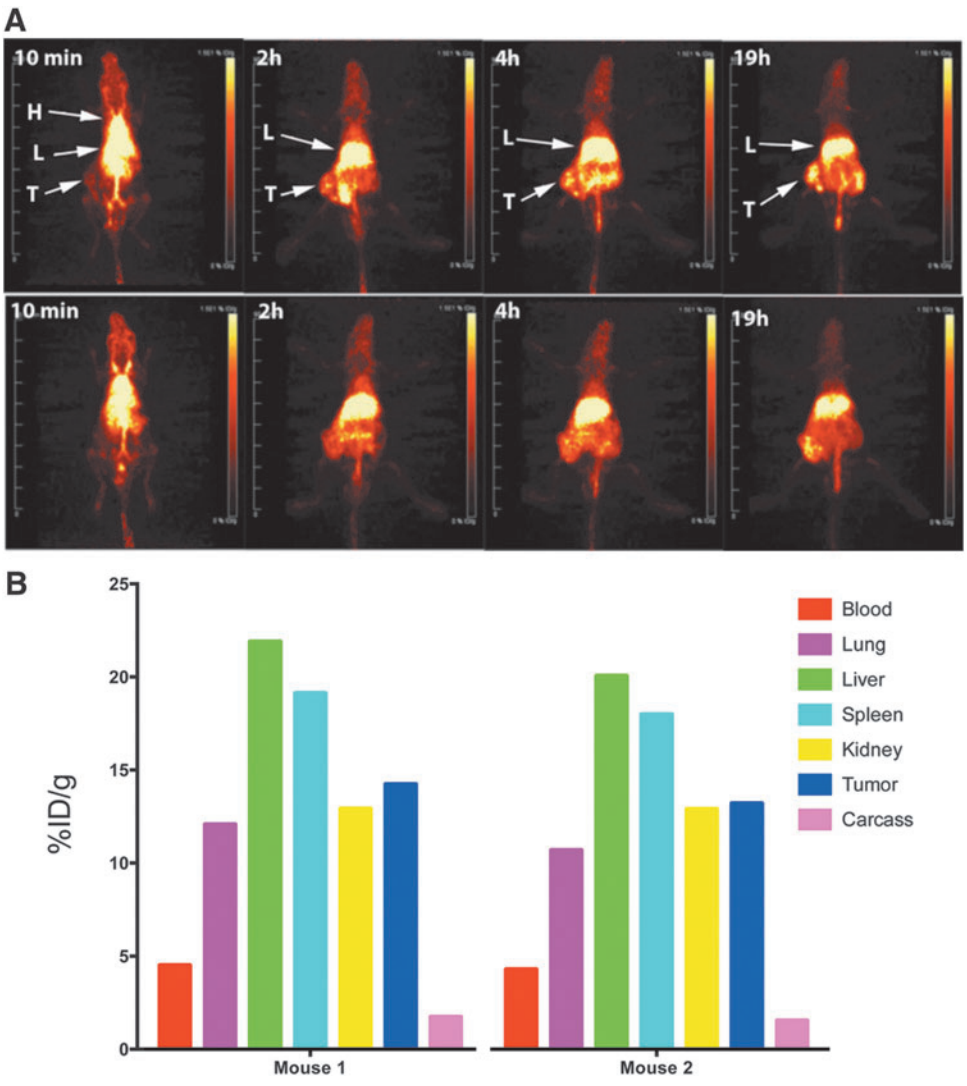

FIG. 8. PET imaging and biodistribution of Dox-LNP mixed with ^{64}Cu-DOTA-cys-DB-LNP. **(A)** PET imaging of Dox-LNP and ^{64}Cu-DOTA-cys-DB-LNP mixture. Dox-LNP was mixed with ^{64}Cu-DOTA-cys-DB-LNP and the mixture was injected into two male NOD/SCID mice bearing LnCap tumors. Serial PET imaging was acquired over the 19 hours time course for both mice. Major organs imaged were heart (H), liver (L), and tumor (T). **(B)** Biodistribution of Dox-LNP and ^{64}Cu-DOTA-cys-DB-LNP mixture. After the final PET image was acquired, mice were euthanized, tissues weighed, and counted for radioactivity for biodistribution analysis. The data are expressed for the two individual mice as % ID/g for major organs at the terminal time point of 19 hours. cys-DB, cys-diabody; LNP, lipid nanoparticle; NOD/SCID, non-obese diabetic severe combined immune deficiency; PET, positron emission tomography.

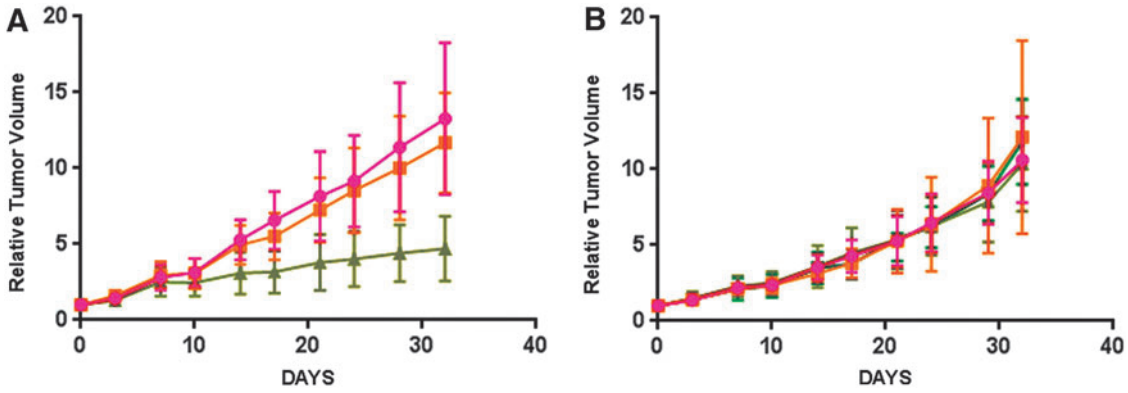

FIG. 9. Treatment of NOD/SCID mice bearing LnCap tumors with drug-LNP plus cys-DB-LNP mixtures or drug cys-DB conjugates. **(A)** Groups of 7–8 male NOD/SCID mice bearing LnCap tumors were treated twice a week for 4 weeks with saline (*red circles*), cys-DB-LNP plus Dox-LNP (*orange squares*) or cys-DB-LNP plus MMAE-LNP (*green triangles*) and relative tumor volume measured twice a week. **(B)** Groups of 7–8 male NOD/SCID mice bearing LnCap tumors were treated twice a week for 4 weeks with saline (*red circles*), cys-DB 5.0 mg/kg (*orange squares*), 2.5 mg/kg of MMAE-cys-DB (*dark-green triangles*) or 5.0 mg/kg MMAE-cys-DB (*light-green triangles*) and relative tumor volume measured twice a week. cys-DB, cys-diabody; LNP, lipid nanoparticle; NOD/SCID, non-obese diabetic severe combined immune deficiency.

fluorescent and easy to detect both *in vitro* and *in vivo*. Using PET imaging, we progressively show increasing tumor drug uptake in our model system starting from ^{64}Cu-64-DOTA-Dox (2%–3% ID/g) to ^{64}Cu-DOTA-Dox-LNP (10% ID/g), and finally to a mixture of two LNPs, a Dox-LNP and a DOTA-cys-DB-LNP (15% ID/g). As a starting point, we showed that a mixture of noncovalent Dox plus LNP performed no better than free Dox; that is, Dox +LNP *in vivo* rapidly lost Dox to a Dox-serum albumin complex showing instability. Thus, free Dox versus Dox + LNP had similar tumor uptake, even though the error bar is greater for Dox + LNP. As a result, we pursued covalent attachment of Dox to overcome this problem. As predicted, the covalent Dox-LNP performed better in tumor uptake.

Compared with ADCs, this approach has a distinct advantage, namely only one antibody-LNP conjugate needs to be prepared that can be later mixed with a wide variety of drug-LNP conjugates. Thus, a patient may be treated with multiple drugs using a single targeting agent or a single drug with multiple targeting agents or both combinations. To validate our approach, we now need to perform therapeutic studies and determine if the LNP conjugate mixtures perform better than conventional drug therapy and result in less normal tissue toxicity.

We go on, in a limited trial, to demonstrate the potential of the targeted LNP drug mixtures in a therapeutic model. Although the Dox-LNP plus cys-DB-LNP mixture showed no tumor reduction, an alternate drug, MMAE-LNP plus cys-DB-LNP did, demonstrating the importance of matching the drug to the type of tumor.

Notably, MMAE ADCs have given clinical responses,[39,40] suggesting that this class of drug (antimicrotubule agents) may be more appropriate as immunoconjugates. However, in this study, the direct conjugate of MMAE to cys-DB showed no tumor reduction even when tested at two-dose levels. Thus, the LNP format is more potent than the drug-cys-DB format. Since auristatin alone as a drug causes significant side effects,[38] its conjugation to antibodies, or in this case to LNPs, reduces toxicity. Although a reversible liver toxicity was observed in the LNP format, the weight loss can likely be reduced by administration of an antinausea medication, similar to the strategy used in human studies.

Since the major goal of this study was to produce covalent LNP mixtures that incorporated both drugs and a targeting agent, we limited the therapy study to a proof of principle. Future studies will be directed at optimization of the drug-LNP plus targeting-LNP ratios and dose response. The strength of our approach was the use of PET imaging to quantitatively demonstrate blood clearance, normal tissue uptake, and tumor targeting at each stage of development.

Acknowledgments

The authors thank the City of Hope Electron Microscope Core Facility, whose use of the FEI Tecnai 12 transmission electron microscope was provided by Office of Naval Research N00014-02-1 0958. Research reported in this publication included work performed in the Small Animal Imaging Core supported by the National Cancer Institute of the National Institutes of Health under award number P30CA33572. The content is solely the responsibility of the authors and does not necessarily represent the official views of the National Institutes of Health. Support from the Charles Reames Family (to J.W.) is gratefully acknowledged.

Disclosure Statement

No competing financial interests exist.

References

1. Kraft JC, Freeling JP, Wang Z, et al. Emerging research and clinical development trends of liposome and lipid nanoparticle drug delivery systems. J Pharm Sci 2014;103:29.
2. Musacchio T, Torchilin VP. Recent developments in lipid-based pharmaceutical nanocarriers. Front Biosci (Landmark Ed) 2011;16:1388.
3. Torchilin VP. Multifunctional, stimuli-sensitive nanoparticulate systems for drug delivery. Nat Rev Drug Discov 2014; 13:813.
4. Allen TM, Cullis PR. Liposomal drug delivery systems: From concept to clinical applications. Adv Drug Deliv Rev 2013;65:36.

5. Pattni BS, Chupin VV, Torchilin VP. New developments in liposomal drug delivery. Chem Rev 2015;115:10938.
6. Torchilin VP. Lipid-core micelles for targeted drug delivery. Curr Drug Deliv 2005;2:319.
7. Movassaghian S, Merkel OM, Torchilin VP. Applications of polymer micelles for imaging and drug delivery. Wiley Interdiscip Rev Nanomed Nanobiotechnol 2015; 7:691.
8. Sawant RR, Torchilin VP. Polymeric micelles: Polyethylene glycol-phosphatidylethanolamine (PEG-PE)-based micelles as an example. Methods Mol Biol 2010; 624:131.
9. Wang Y, Wang R, Lu X, et al. Pegylated phospholipids-based self-assembly with water-soluble drugs. Pharm Res 2010;27:361.
10. Sriraman SK, Aryasomayajula B, Torchilin VP. Barriers to drug delivery in solid tumors. Tissue Barriers 2014; 2:e29528.
11. Greish K. Enhanced permeability and retention (EPR) effect for anticancer nanomedicine drug targeting. Methods Mol Biol 2010;624:25.
12. Maeda H, Wu J, Sawa T, et al. Tumor vascular permeability and the EPR effect in macromolecular therapeutics: A review. J Control Release 2000;65:271.
13. Maeda H. Tumor-selective delivery of macromolecular drugs via the EPR effect: Background and future prospects. Bioconjug Chem 2010;21:797.
14. Sawant RR, Jhaveri AM, Torchilin VP. Immunomicelles for advancing personalized therapy. Adv Drug Deliv Rev 2012;64:1436.
15. Wittrup KD, Thurber GM, Schmidt MM, et al. Practical theoretic guidance for the design of tumor-targeting agents. Methods Enzymol 2012;503:255.
16. Ranjan S, Sood R, Dudas J, et al. Peptide-mediated targeting of liposomes to TrkB receptor-expressing cells. Int J Nanomedicine 2012;7:3475.
17. Schmidt MM, Wittrup KD. A modeling analysis of the effects of molecular size and binding affinity on tumor targeting. Mol Cancer Ther 2009;8:2861.
18. Kirpotin DB, Drummond DC, Shao Y, et al. Antibody targeting of long-circulating lipidic nanoparticles does not increase tumor localization but does increase internalization in animal models. Cancer Res 2006;66:6732.
19. Torchilin VP. Micellar nanocarriers: Pharmaceutical perspectives. Pharm Res 2007;24:1.
20. Ristau BT, O'Keefe DS, Bacich DJ. The prostate-specific membrane antigen: Lessons and current clinical implications from 20 years of research. Urol Oncol 2014;32:272.
21. Elgqvist J. Nanoparticles as theranostic vehicles in experimental and clinical applications-focus on prostate and breast cancer. Int J Mol Sci 2017;18:E1102.
22. Barve A, Jin W, Cheng K. Prostate cancer relevant antigens and enzymes for targeted drug delivery. J Control Release 2014;187:118.
23. van der Geest T, Laverman P, Metselaar JM, et al. Radionuclide imaging of liposomal drug delivery. Expert Opin Drug Deliv 2016;13:1231.
24. Goel S, England CG, Chen F, et al. Positron emission tomography and nanotechnology: A dynamic duo for cancer theranostics. Adv Drug Deliv Rev 2016;113:157.
25. Pratt EC, Shaffer TM, Grimm J. Nanoparticles and radiotracers: Advances toward radionanomedicine. Wiley Interdiscip Rev Nanomed Nanobiotechnol 2016;8:872.
26. Chakravarty R, Goel S, Dash A, et al. Radiolabeled inorganic nanoparticles for positron emission tomography imaging of cancer: An overview. Q J Nucl Med Mol Imaging 2017;61:181.
27. Wong P, Li L, Chea J, et al. PET imaging of ^{64}Cu-DOTA-scFv-anti-PSMA lipid nanoparticles (LNPs): Enhanced tumor targeting over anti-PSMA scFv or untargeted LNPs. Nucl Med Biol 2017;47:62.
28. Shen F, Chu S, Bence AK, et al. Quantitation of doxorubicin uptake, efflux, and modulation of multidrug resistance (MDR) in MDR human cancer cells. J Pharmacol Exp Ther 2008;324:95.
29. Smith-Jones PM, Vallabahajosula S, Goldsmith SJ, et al. *In vitro* characterization of radiolabeled monoclonal antibodies specific for the extracellular domain of prostate-specific membrane antigen. Cancer Res 2000;60:5237.
30. Li L, Turatti F, Crow D, et al. Monodispersed DOTA-PEG-conjugated anti-TAG-72 diabody has low kidney uptake and high tumor-to-blood ratios resulting in improved ^{64}Cu PET. J Nucl Med 2010;51:1139.
31. Yazaki PJ, Clark C, Shively L, et al. Mammalian expression and hollow fiber bioreactor production of recombinant anti-CEA diabody and minibody for clinical applications. J Immunological Methods 2001;253:195.
32. Lewis MR, Kao JY, Anderson AL, et al. An improved method for conjugating monoclonal antibodies with N-hydroxysulfosuccinimidyl DOTA. Bioconjug Chem 2001; 12:320.
33. Mortimer JE, Bading JR, Colcher DM, et al. Functional imaging of human epidermal growth factor receptor 2-positive metastatic breast cancer using (64)Cu-DOTA-trastuzumab PET. J Nucl Med 2014;55:23.
34. Swenson CE, Bolcsak LE, Batist G, et al. Pharmacokinetics of doxorubicin administered i.v. as Myocet (TLC D-99; liposome-encapsulated doxorubicin citrate) compared with conventional doxorubicin when given in combination with cyclophosphamide in patients with metastatic breast cancer. Anticancer Drugs 2003;14:239.
35. Freyer G, Tranchand B, Ligneau B, et al. Population pharmacokinetics of doxorubicin, etoposide and ifosfamide in small cell lung cancer patients: Results of a multicentre study. Br J Clin Pharmacol 2000;50:315.
36. Bronchud MH, Margison JM, Howell A, et al. Comparative pharmacokinetics of escalating doses of doxorubicin in patients with metastatic breast cancer. Cancer Chemother Pharmacol 1990;25:435.
37. Saraiva C, Praca C, Ferreira R, et al. Nanoparticle-mediated brain drug delivery: Overcoming blood-brain barrier to treat neurodegenerative diseases. J Control Release 2016;235:34.
38. Alley SC, Zhang X, Okeley NM, et al. The pharmacologic basis for antibody-auristatin conjugate activity. J Pharmacol Exp Ther 2009;330:932.
39. McCombs JR, Owen SC. Antibody drug conjugates: Design and selection of linker, payload and conjugation chemistry. AAPS J 2015;17:339.
40. Schumacher D, Hackenberger CP, Leonhardt H, et al. Current status: Site-specific antibody drug conjugates. J Clin Immunol 2016;36(Suppl 1):100.